Applied Energy 327 (2022) 120035

Contents lists available at ScienceDirect

Applied Energy

journal homepage: www.elsevier.com/locate/apenergy

Bidding strategy for wireless charging roads with energy storage in real-time electricity markets

Jie Shi [a], Nanpeng Yu [b], H. Oliver Gao [a,*]

[a] Department of Systems Engineering, Cornell University, Ithaca, NY, 14850, USA
[b] Department of Electrical and Computer Engineering, University of California, Riverside, CA, 92521, USA

GRAPHICAL ABSTRACT

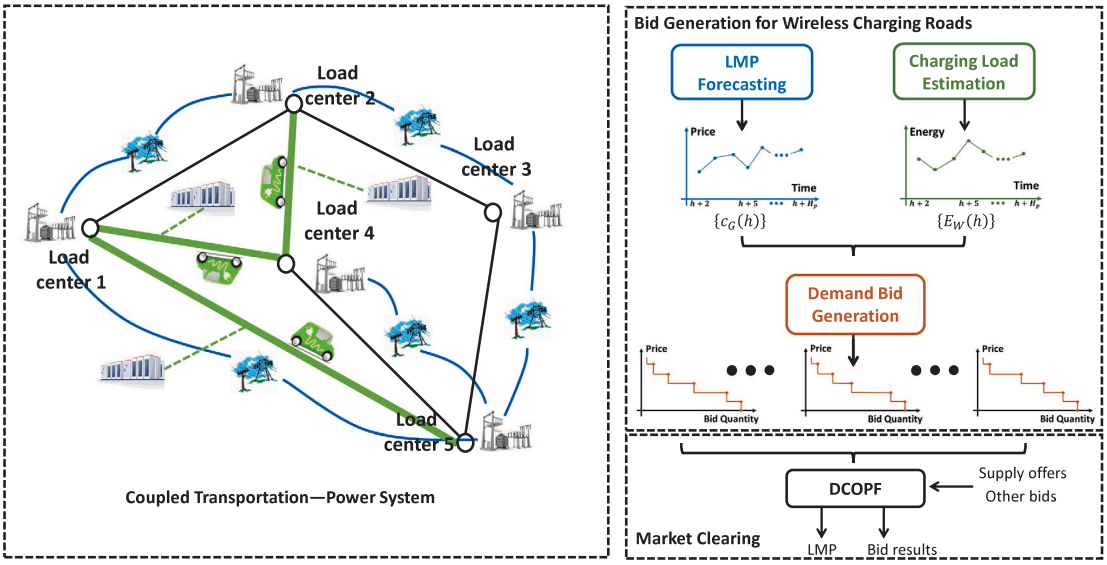

ARTICLE INFO

Keywords:
Electric vehicle
Energy storage system
Wireless charging road
Point queue model
Electricity market
Demand bid
Optimal power flow
Model predictive control
Locational marginal price forecasting

ABSTRACT

The combination of wireless charging roads and energy storage systems is a promising option for electric vehicle charging because of their capabilities in mitigating range anxiety of electric vehicle drivers. Wireless charging road operators can purchase electric energy by submitting price-sensitive demand bids in real-time electricity markets. Efficient bidding strategies are crucial to minimizing the energy costs for providing wireless charging services. In this study, we first propose a composite statistical model based on graph signal processing and linear regression to forecast the future locational marginal prices (LMPs) in a power network. Then an estimate of future electric load on each wireless charging road is derived by simulating its traffic flow using a point queue-based traffic flow model. An efficient price-sensitive bidding strategy for each individual wireless charging road is developed based on its LMP forecast, wireless charging load estimate, and a model predictive control framework. Our numerical example shows that the proposed price-sensitive demand bidding strategy

* Corresponding author.
E-mail address: hg55@cornell.edu (H.O. Gao).

https://doi.org/10.1016/j.apenergy.2022.120035
Received 23 January 2022; Received in revised form 18 September 2022; Accepted 21 September 2022
Available online 5 October 2022

reduces the electric energy cost for operating a wireless charging road with an energy storage system by 6% compared to a baseline bidding strategy.

1. Introduction

Range anxiety, according to Voelcker [1], is one of the main reasons hindering a broader adoption of electric vehicles (EVs). Though efforts are constantly being made to increase both battery capacity and energy efficiency, EVs on the market today still face a significantly lower range than their internal combustion engine (ICE) counterparts. Moreover, recharging an EV in a charging station still consumes much more time than refueling an ICE vehicle in a gas station [2]. A typical L2 charger, which is the most popular charging facility for daily EV usage, has a charging speed of only around 25 miles per charging hour [3].

A potential solution to EV range anxiety would be the widespread adoption of wireless charging roads, allowing EVs to travel and recharge simultaneously, notably extending their effective ranges. Recent research and pilot projects have demonstrated the practicality of wireless charging roads. See [4] for a couple of real-world projects carried out by an Israeli company called Electreon. For example, its Smartroad Gotland project [5] builds a wireless electric inter-city road system designed for charging electric buses and heavy trucks. Electreon also works with Stellantis [6], which is the world's fifth-largest automaker, to build and test a loop of road in Italy with wireless charging coils embedded under the surface, so that EVs can charge as they drive [7].

The electric loads of busy wireless charging roads can reach tens of megawatts, making them eligible to participate in real-time electricity markets. To reduce energy cost as well as improve system reliability, an energy storage system (ESS) is highly recommended to be used in conjunction with a wireless charging road. The adoption of ESSs provides wireless charging road operators with flexibility in the quantity of power drawn from power grids, allowing them to submit price-sensitive demand bids in real-time electricity markets. Given electricity prices vary drastically with time, an efficient bidding strategy is crucial in minimizing the energy cost associated with operating a wireless charging road. The goal of this study is to design a competitive price-sensitive demand bidding strategy for wireless charging roads with energy storage to save electricity cost within the context of real-time electricity markets.

As will be shown later, the proposed demand bidding strategy for wireless charging roads not only yields lower energy costs but also imposes less pressure on the existing power grid infrastructure. These two primary merits can bring broad benefits to our society. For example, cost reduction in operating wireless charging roads is likely to attract more investments in construction as well as lowering the corresponding charging prices, thereby promoting the overall EV adoption. Meanwhile, the alleviation of required pressure on power grid is a great news to the power industry, which already suffers significant strains on the existing infrastructure.

Wireless charging roads couple two primary infrastructure sectors together: power and transportation. Previous research has investigated potential issues raised by this emerging coupled transportation–power system characterized by electrified road networks. For instance, optimal strategies for wireless charging road placement are discussed in [8–10], and [11] given various scenarios and assumptions. A novel routing policy is proposed in [12] to provide EV drivers the optimal charging schedule composed of both plug-in chargers and wireless charging roads. Some studies also investigate the impacts of wireless charging roads on existing power infrastructure as well as coordination between power systems and electrified road networks. For example, Manshadi et al. [13] shows that efficiently-coordinated operation of wireless charging roads and power system can reduce congestion within power network, leading to lower electricity prices. Ou et al. [14] studies the impact of wireless charging roads on locational marginal prices (LMPs) in the context of wholesale electricity markets. Xia et al. [15] develops a distributed approach based on mixed integer linear programming to optimally deploy wireless charging roads in a coupled transportation–power system with the objective of revenue maximization. However, none of the above studies address bidding strategy design for wireless charging roads with energy storage (WCRES) to participate in wholesale electricity markets.

Bidding strategies for traditional stakeholders in wholesale electricity markets have received widespread interest in academia. Various efforts have been made to either improve energy producers' profitability or reduce demand-side electricity cost. For instance, Conejo et al. [16] develops a framework to obtain the optimal bidding strategy for a price-taker electricity producer to maximize its expected profit. However, this strategy is only for electricity generator in a pool-based energy market. By contrast, Fleten and Pettersen [17] designs optimal piecewise-linear bidding curves for electricity retailers to minimize their cost to purchase power from wholesale electricity markets. However, independent large-scale load consumers like wireless charging roads are not discussed. Jiang and Powell [18] develops an approximate dynamic programming-based bidding strategy for owners of battery energy storage systems to gain revenues by participating in real-time electricity markets. Their proposed approach requires significant amount of trials and exploration before convergence, which might not be desirable for practical application. Liu et al. [19] and Wei et al. [20] propose model predictive control (MPC) based algorithms to construct efficient block bidding curves for residential building clusters, which reduce their energy costs in the context of electricity markets. However, neither of them consider the participation of energy storage systems. With the increasing popularity of EVs, many researchers support the idea of EV aggregators that collect battery resources from individual EVs as a distributed energy storage system. Various bidding policies are proposed for these EV aggregators to participate in electricity markets [21–26]. However, none of these studies cover strategies for WCRES to bid in wholesale electricity markets. Simple adaption of previous bidding methods does not suffice our problem, which couples transportation systems with power systems. This study aims at designing a competitive price-sensitive demand bidding strategy for wireless charging roads with energy storage, which interacts with both transportation sector and power sector. A proper design of bidding strategies for wireless charging roads needs to take into consideration factors from both the power system and the transportation system, such as LMP forecasts, traffic flow prediction, and driver preference variation caused by lane congestion.

To the best of the authors' knowledge, this is the first study that investigates a bidding strategy for WCRES to participate in real-time wholesale electricity markets. We aim at developing an efficient price-sensitive bidding strategy that helps reduce energy costs accrued by owners of wireless charging road in providing charging services to EVs. The proposed bidding strategy is based on an MPC framework that takes LMP forecasts and wireless charging load estimates as inputs and outputs an optimal bid-quantity price pair. Different bid-quantity price pairs can be derived by running MPC framework with adjusted LMP forecasts. A block bidding curve is then constructed with these bid-quantity price pairs. To this end, we design a spatio-temporal LMP forecasting algorithm and a wireless charging load estimator based on a dynamic traffic assignment model to obtain reliable prediction of future LMPs and electric loads on wireless charging roads,

The main contributions of this study are summarized as follows:

- We propose a composite statistical model based on graph signal processing and linear regression to spatio-temporally forecast locational marginal prices at different nodes in a given power

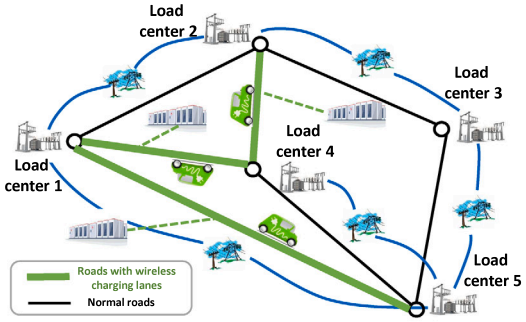

(a) Coupled transportation–power system.

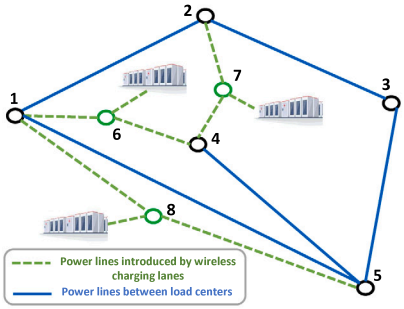

(b) Power network.

Fig. 1. Transportation–power system with five load centers and three wireless charging roads.

network. The proposed model, though with fewer parameters, achieves higher forecast accuracy than the vector autoregressive-based models in our numerical example.

- We develop a wireless charging load estimator by simulating EV traffic flow dynamics based on a point queue model for each wireless charging road. The proposed approach is able to predict the electric load on a wireless charging road network within the near future.
- We design an efficient price-sensitive bidding strategy based on a model predictive control framework for a wireless charging road to participate in the real-time electricity market. The proposed bidding strategy not only reduces the energy cost for operating a wireless charging road but also helps alleviate electric load pressure on a power network.

The rest of this paper is organized as follows: Section 2 illustrates the problem setting and the overall framework of the proposed price-sensitive bidding strategy. Section 3 elaborates on the technical details, including the GSP-based LMP forecasting, the wireless charging load estimation, and the MPC-based demand bid curve generation. Section 4 demonstrates the effectiveness of the proposed price-sensitive bidding strategy by carrying out a numerical example. The conclusions are stated in Section 5.

2. Problem setting and overall framework

Below we present the problem setting and describe the goal of this study, which is followed by a discussion of the overall framework of the proposed price-sensitive bidding strategy for WCRES systems.

2.1. Problem setting

In this study, we consider a coupled transportation–power system that includes one or more wireless charging roads. Each wireless charging road is equipped with an ESS that enables energy arbitrage. Fig. 1(a) shows an example of a coupled transportation–power system comprised of five load centers. Throughout this paper, a load center denotes a region with intensive human activities, for example, a town or a city. The load centers are connected by a road network and a power network. As displayed in Fig. 1(a), the black and green lines represent normal roads and wireless charging roads, respectively. Note that a wireless charging road can consist of both normal lanes and wireless charging lanes, but only EVs that require charging service are allowed to travel on the wireless charging lanes. Meanwhile, the load centers are also interconnected by transmission lines (the blue curves in Fig. 1(a)) in the power network.

Throughout this study, we treat each wireless charging road as an individual bus in the power network, which is linked to the two load centers it connects. Fig. 1(b) illustrates the complete power network extracted from the original coupled transportation–power system. Bus 6, 7, and 8 (green circles) represent the wireless charging roads, which are connected to their adjacent buses through additional power lines (green dashed lines). As discussed in the introduction, wireless charging roads consume a large amount of electric power, making them eligible to participate in real-time wholesale electricity markets. The objective of this study is to design an efficient bidding strategy for individual wireless charging roads to reduce energy costs for providing EV charging services.

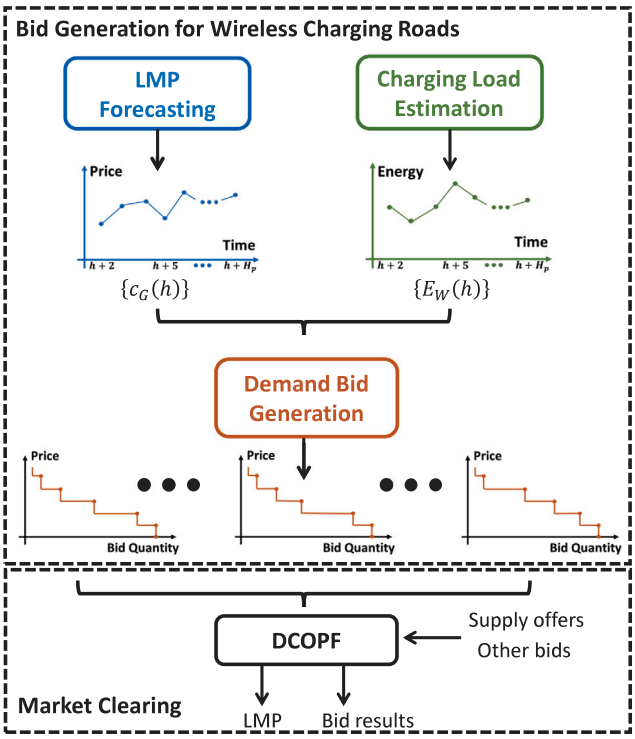

Fig. 2. Overall framework of the proposed bid generation process and market clearing.

2.2. Overall framework

Fig. 2 depicts the overall framework of the proposed bid generation process and electricity market clearing. The proposed bidding strategy for a wireless charging road comprises three primary modules: LMP forecasting, wireless charging load estimation, and demand bid generation. The outputs of the first two modules serve as the inputs of the last module. We only present a high-level description of each module below and present their technical details in the next section.

A locational marginal price is basically the price of electric energy being sold at a particular location. It usually consists of three components: marginal energy price, marginal congestion price, and marginal loss price. The energy price component is primarily dependent on the bids submitted by the power generation companies. It could be affected by multiple factors such as the costs of fuel and supply–demand imbalance. The congestion price is caused by the capacity constraints of the power infrastructure. This component can get quite large during peak hours. Loss price captures the electric energy loss cost during the power transmission. In a word, LMP is a quite sensitive variable that depends on various factors, which can change frequently even within a day.

The goal of the LMP forecasting module is to provide accurate prediction of electricity prices at a wireless charging road in the near future. In this study, a composite statistical model based on graph signal processing (GSP) and linear regression is developed to forecast future electricity prices. The proposed regression model takes LMP at previous hour, temperature forecast, and time indices as inputs and outputs an estimate of the LMP for the next hour. LMP forecasts at subsequent hours can be obtained by applying the proposed regression model iteratively. Note that the prediction horizon starts at $h+2$ which is two hours into the future from current hour as shown in Fig. 2. The reason is that many real-time wholesale electricity operators in the United States, for example, the California Independent System Operator (CAISO) and the New York Independent System Operator (NYISO), require participants to submit their energy bids 75 min before the start of the trading hour.

The wireless charging load estimation module is designed to produce accurate estimates of electric loads within the near future. In this study, we assume estimates of future inflows of EVs and traditional vehicles are available to wireless charging roads. Note that EVs have different probabilities in selecting wireless charging lanes under different traffic conditions. A point queue-based model is developed to model the dynamics of traffic flow on a wireless charging road. The accumulated traffic on both normal lanes and wireless charging lanes in future hours can be simulated based on the inflow estimates and the proposed traffic flow model. The wireless charging load at a certain time step is therefore estimated by multiplying the number of EVs and charging power per vehicle. We will elaborate on the technical details of the wireless charging load estimation module in Section 3.2.

The objective of the demand bid generation module is to provide an efficient price-sensitive bidding strategy for a wireless charging road owner that participates in a real-time wholesale electricity market. This module takes the LMP forecasts and the wireless charging load estimates as inputs and outputs a block bid that describes the relationship between electricity price and bid quantity. The knots (price–quantity pairs) in the block bid are derived from an optimization process based on model predictive control. Note that there can be a minimum bid quantity that is greater than zero when the maximum output of the corresponding ESS does not match the wireless charging load. In this case, the minimum bid quantity can be considered as a fixed bid, regardless of the electricity price. The detailed methodology regarding demand bid generation will be discussed in Section 3.3.

The lower part of Fig. 2 illustrates the key components of the clearing process of demand bids and supply offers in a typical wholesale electricity market. Most independent system operators (ISOs) and regional transmission organizations (RTOs) adopt algorithms based on optimal power flow (OPF) to settle transactions and calculate clearing prices, which are exactly LMPs in the power grid. As shown in Fig. 2, the inputs of DC OPF (DCOPF) in our case are supply offers from generation resources and demand bids from wireless charging roads and other load centers. The outputs of DCOPF are market clearing results and LMPs at different nodes in the power grid.

Remark. Note the primary goal of this paper is to provide a potential algorithmic bidding solution for future integration of wireless charging roads into the existing electricity markets. The real-world system could be much more complicated than what we present in this study. The performance of the proposed bidding algorithm, when applied in practice, will be affected by traffic condition, infrastructure quality, weather, scale of wireless charging roads and load centers, etc.

3. Methodologies

In this section, we present the technical details of the modules introduced in the overall framework. We start with a full discussion of the GSP-based regression model for LMP forecasting, which is followed by an illustration of a point queue-based traffic flow model for wireless charging load estimation. Next, we elaborate on the MPC-based demand bid generation for individual wireless charging roads. This section ends with brief coverage of DCOPF.

3.1. LMP forecasting

The LMP forecasting plays a critical role in determining the price-sensitive demand bid. An accurate prediction of future LMPs is a prerequisite for successful energy cost saving. To this end, we develop a spatio-temporal regression model based on the GSP to forecast hourly LMPs at different nodes in a given power network.

3.1.1. Regression model

Let $y_i(h)$ be the ith node's LMP at hour h. Let $T_i(h)$ denote the temperature of the ith node at hour h. Let $I(h) = \sin\frac{\pi h}{12}$ be the time index of hour h. The sine function is adopted to normalize time and smooth the transition between 23:00 and 0:00. Then our regression model for LMP forecasting is formulated by:

$$y_i(h) = \underbrace{\beta_{i,1}y_i(h-1) + \beta_{i,2}y_i(h-24)}_{\text{Historic LMP}} + \underbrace{\beta_{i,3}T_i(h) + \beta_{i,4}T_i^2(h) + \beta_{i,5}T_i^3(h)}_{\text{Temperature}} + \underbrace{\beta_{i,6}I(h) + \beta_{i,7}I^2(h)}_{\text{Time index}} + \underbrace{\epsilon_i(h)}_{\text{Error}}, \tag{1}$$

where $\epsilon_i(h)$ denotes the error term. $\{\beta_{i,1}, \ldots, \beta_{i,7}\}$ are the coefficients to be estimated. The covariates on the right hand side are categorized into three groups, which contain the information of historic LMP, temperature, and time, respectively. These features are considered to be highly correlated with $y_i(h)$. For example, an LMP at one time step is usually close to its predecessor. We adopt $y_i(h-24)$ into our model because there is a strong daily pattern of seasonality. Note that $T_i^2(h)$, $T_i^3(h)$, and $I^2(h)$ are introduced to account for a potential nonlinear relationship between LMP, temperature, and the time index.

LMPs at different nodes in a power network can be considered as a multivariate time series $\boldsymbol{y}(h) = [y_1(h), \ldots, y_N(h)]^\top$, where N denotes the number of nodes. Eq. (1) captures the temporal correlation within individual LMP time series by adopting autoregressive terms $\beta_{i,1}y_i(h-1)$ and $\beta_{i,2}y_i(h-24)$. However, the spatial correlation between different nodes is not explicitly modeled, leaving the information of spatial dependence within the error terms from individual regression models. To improve the prediction accuracy, we propose a GSP-based approach that exploits the spatial correlation between error terms.

3.1.2. Model error terms as graph signal

In this subsection, we model the error terms of individual regression models as a graph signal. Let $\boldsymbol{\epsilon}(h) = [\epsilon_1(h), \ldots, \epsilon_N(h)]^\top$ denote the vector of error terms at hour h. An undirected spatial graph $G_S = (\mathcal{V}_S, \mathcal{E}_S)$ corresponding to $\boldsymbol{\epsilon}(h)$ can be constructed based on the power network topology. In addition, an undirected line graph $G_L = (\mathcal{V}_\mathcal{L}, \mathcal{E}_\mathcal{L})$ is built to model $\boldsymbol{\epsilon}(h)$'s dependence on $\boldsymbol{\epsilon}(h-1)$ and $\boldsymbol{\epsilon}(h-24)$. By performing a Cartesian product of G_S and G_L, we obatain a product graph $G_P = (\mathcal{V}_\mathcal{P}, \mathcal{E}_\mathcal{P})$ that models the spatio-temporal dependence between individual error terms:

$$G_P = G_S \square G_L \tag{2}$$

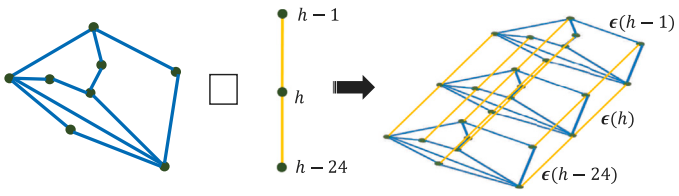

Fig. 3. Cartesian product of a spatial graph representing the eight-node power network and a line graph representing temporal dependence.

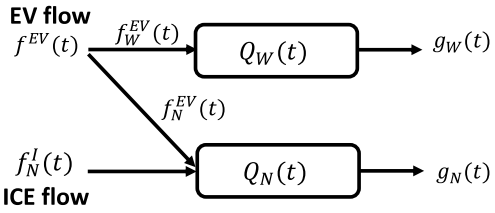

Fig. 4. Overall framework of the proposed point queue-based traffic flow model.

Fig. 3 illustrates a product graph derived from the Cartesian product of a spatial graph representing the eight-node power network shown in Fig. 1(b) and a line graph representing temporal dependence between $\epsilon(h-1)$, $\epsilon(h)$, and $\epsilon(h-24)$.

Let A, A_S, and A_L denote the adjacency matrices of graphs G_P, G_S, and G_L. A_{ij} equals 1 if nodes i and j are connected by an edge, 0 otherwise. Given A_S and A_L, we can calculate A using the following equation:

$$A = I_L \otimes A_S + A_L \otimes I_S, \tag{3}$$

where I_L and I_S are identity matrices with sizes equal to the numbers of vertices in G_L and G_S, respectively. The corresponding graph Laplacian of adjacency matrix A can be derived by:

$$L = D - A, \tag{4}$$

where D is a diagonal matrix with $D_{ii} = \sum_j A_{ij}$. As will be shown soon, graph Laplacian L is a fundamental term for error term estimation.

3.1.3. Estimation of the error terms

Given a graph signal of error terms, our goal is to estimate $\epsilon(h)$ based on known values of $\epsilon(h-1)$ and $\epsilon(h-24)$. Let $\boldsymbol{s} = [\epsilon(h-1)^\top, \epsilon(h)^\top, \epsilon(h-24)^\top]^\top$ denote the entire graph signal. We can convert $\boldsymbol{s}$ into its Laplacian spectral domain by performing the graph Fourier transform (GFT) [27]:

$$\boldsymbol{S} = U^{-1}\boldsymbol{s}, \tag{5}$$

where $\boldsymbol{S} = \left[S(1), \ldots, S(N_G)\right]$ is a vector consisting of Laplacian spectral components. $N_G = 3N$ denotes the number of vertices in G_P. U is a matrix comprised of eigenvectors of graph Laplacian L. These eigenvectors in U are sorted in an ascending order according to their corresponding eigenvalues. Note that L is positive semi-definite by definition with its eigenvalues being non-negative. The spectral components in $\boldsymbol{S}$ that correspond to smaller/larger eigenvalues of L are lower/higher frequency components. The inverse graph Fourier transform (IGFT) is defined by:

$$\boldsymbol{s} = U\boldsymbol{S}. \tag{6}$$

Our graph signal $\boldsymbol{s}$ is expected to be of low-pass type because of the spatio-temporal dependence between the error terms. We assume the first N_P spectral components capture the majority of the information in $\boldsymbol{s}$, where $N_P \leq 2N$. Based on the IGFT, we can solve $\boldsymbol{S}_P = \left[S(1), \ldots, S(N_P)\right]$ by:

$$\boldsymbol{S}_P = U_M^*(U_M U_M^*)^{-1} \cdot \boldsymbol{s}_K, \tag{7}$$

where $\boldsymbol{s}_K$ denotes the $2N$ known values (historic error terms) in $\boldsymbol{s}$. U_M collects the first N_P columns in U with only the $2N$ rows that correspond to $\boldsymbol{s}_K$ being left. Therefore, the dimension of U_M is $2N$ by N_P. Then, the entire graph signal can be reconstructed as:

$$\hat{\boldsymbol{s}} = U_P\boldsymbol{S}_P, \tag{8}$$

where U_P is a matrix of the eigenvectors of L that correspond to the first N_P spectral components. An estimate of $\epsilon(h)$ is therefore obtained by extracting the corresponding elements from $\hat{\boldsymbol{s}}$.

The LMPs at different nodes in the near future can be predicted by iteratively applying the regression model and error term estimation. Note that the temperature forecasts at different nodes are assumed to be available throughout this study.

3.2. Wireless charging load estimation

Wireless charging load in the near future on a wireless charging road needs to be estimated for building the price-sensitive demand bid curve. We assume the charging power of each EV is fixed and remains the same across operating hours. Therefore, the wireless charging load is proportional to the number of EVs on the wireless charging lanes. In this subsection, we develop a point queue-based traffic flow model to simulate the dynamics of a given wireless charging road. The numbers of EVs on the wireless charging lanes in upcoming hours can therefore be estimated from the simulated traffic flow.

Fig. 4 illustrates the overall framework of the proposed point queue-based traffic flow model. We consider a wireless charging road consisting of both wireless charging lanes and normal lanes. EVs can select either one of them at the entrance of the road. ICE vehicles can only travel on normal lanes at any time. Let two point queues $Q_W(t)$ and $Q_N(t)$ represent the total number of vehicles on wireless charging lanes and normal lanes, respectively. $f^{EV}(t)$ denotes the inflow of EVs to the entire wireless charging road. $f_W^{EV}(t)$ and $f_N^{EV}(t)$ represent the upstream influxes of EVs to wireless charging lanes and normal lanes at time step t, respectively. Clearly the following relationship holds at each time step:

$$f^{EV}(t) = f_W^{EV}(t) + f_N^{EV}(t) \tag{9}$$

Let $f_N^I(t)$ denote the inflow of ICE vehicles to normal lanes at time step t. $g_W(t)$ and $g_N(t)$ denote the downstream out-fluxes of vehicles from wireless charging lanes and normal lanes at time step t, respectively. In our proposed model, $g_W(t)$ and $g_N(t)$ are defined as:

$$g_W(t) = \min\left(\frac{Q_W(t)}{T_F}, C_W\right) \tag{10}$$

$$g_N(t) = \min\left(\frac{Q_N(t)}{T_F}, C_N\right), \tag{11}$$

where T_F denotes the free-flow time. The wireless charging lanes and the normal lanes are assumed to have the same free-flow time. C_W and C_N are the total capacities of the wireless charging lanes and the normal lanes, respectively.

The dynamics of $Q_W(t)$ and $Q_N(t)$ are expressed by the following difference equations:

$$Q_W(t+1) = Q_W(t) + \left(f_W^{EV}(t) - g_W(t)\right) \cdot \Delta T \tag{12}$$

$$Q_N(t+1) = Q_N(t) + \left(f_N^{EV}(t) + f_N^I(t) - g_N(t)\right) \cdot \Delta T, \tag{13}$$

where $\Delta T \ll T_F$ is the time interval between two adjacent time steps. Note that both $Q_W(t)$ and $Q_N(t)$ are always non-negative. Let $T_W(t)$ and $T_N(t)$ be the queueing time [28] for $Q_W(t)$ and $Q_N(t)$, respectively. Queueing time measures the additional travel time caused by traffic congestion. $T_W(t)$ and $T_N(t)$ are calculated by:

$$T_W(t) = \max\left(\frac{Q_W(t)}{C_W} - T_F, 0\right) \tag{14}$$

$$T_N(t) = \max\left(\frac{Q_N(t)}{C_N} - T_F, 0\right). \tag{15}$$

The time length of a vehicle traveling through a given wireless charging road equals the sum of the free-flow time and the corresponding queueing time.

EVs can select either wireless charging lanes or normal lanes at the road entrance. The following logit model is adopted to derive the proportion of EVs that select wireless charging lanes at time step t:

$$P_{SWL}(t) = \frac{1}{1 + \exp\left(\alpha(c_W(t) - c_N(t))\right)}, \tag{16}$$

where $c_W(t)$ and $c_N(t)$ denote the costs of EVs traveling through wireless charging lanes and normal lanes, respectively, when entering the wireless charging road at time step t. α is a hyperparameter. Not surprisingly, if $c_W(t)$ and $c_N(t)$ are equal, then half of the EVs will select the wireless charging lanes in our model. In this study, $c_W(t)$ and $c_N(t)$ are defined as follows:

$$c_W(t) = \left(p_W(t) + p_T - p_B\right)\frac{T_W(t) + T_F}{T_F} \tag{17}$$

$$c_N(t) = \frac{p_T\left(T_N(t) + T_F\right)}{T_F}, \tag{18}$$

where p_T is the value of time (VOT). $p_W(t)$ denotes the price of wireless charging at time step t. p_B is the bonus value of selecting wireless charging for an EV. Both $c_W(t)$ and $c_N(t)$ are proportional to their corresponding total travel time. Note that the total travel time is normalized by dividing the free-flow time.

Given inflow of EVs to the wireless charging road $f^{EV}(t)$ and the corresponding $P_{SWL}(t)$, we can estimate $f_W^{EV}(t)$ based on the following equation:

$$f_W^{EV}(t) = P_{SWL}(t) \cdot f^{EV}(t). \tag{19}$$

The number of EVs on the wireless charging lanes within the near future can be simulated by iteratively running the dynamic equation of $Q_W(t)$ (Eq. (12)). Therefore, the wireless charging load at hour h can be estimated by:

$$E_W(h) = \sum_{t=h\cdot N_h+1}^{(h+1)\cdot N_h} P_C \cdot Q_W(t) \cdot \Delta T, \tag{20}$$

where P_C is the wireless charging power for each EV. ΔT is the length of time interval for traffic flow simulation. N_h denotes the number of time intervals within one hour.

3.3. Demand bid curve construction

Demand side participants are allowed to submit price-sensitive bids into real-time wholesale electricity markets in the United States. The wireless charging roads equipped with energy storage systems have strong flexibility in drawing power from the grid, making them ideal entities for submitting price-sensitive demand bids. They can reduce their overall energy costs by taking advantage of time-varying electricity price. Specifically, excessive electric energy is expected to be purchased from the grid and stored into the ESS during nighttime hours with relatively low electricity prices. The stored energy is then released to serve part or all of the wireless charging demand from EVs when the electricity price rises during daytime hours. This scheduling and operation of energy storage devices for energy cost reduction is formally called energy arbitrage.

In this subsection, we develop an efficient bidding strategy based on MPC framework. Our goal is to minimize the energy cost for operating a wireless charging road through efficient energy arbitrage. Given the LMP forecasts and wireless charging load estimates derived from the previous two subsections, we can formulate and solve the following optimization problem to obtain the optimal power drawn from the grid at each hour in the prediction horizon:

$$\underset{P_G(t)}{\text{minimize}} \quad \sum_{h=H_s}^{H_s+H_P-1} P_G(h) \cdot c_G(h) \cdot \Delta H \tag{21}$$

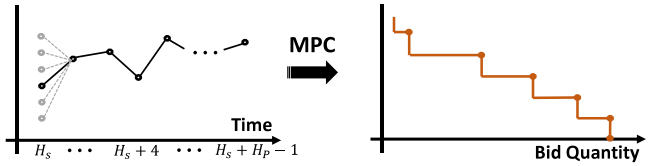

Fig. 5. Demand bid curve generation.

Algorithm 1 Demand bid curve construction for a given wireless charging road.

1: LMP forecast $\boldsymbol{c} = [c_G(H_s), \cdots, c_G(H_s + H_P - 1)]$
2: Wireless charging load estimate $\boldsymbol{e} = [E_W(H_s), \cdots, E_W(H_s + H_P - 1)]$
3: Initialize an empty list for storing price–demand pairs $L_{PD} = []$
4: **for** n in $[-N_c, -N_c + 1, \cdots, N_c]$ **do**
5: Modified LMP forecast $\boldsymbol{c} = [c_G(H_s) + n \cdot \Delta c, \cdots, c_G(H_s + H_P - 1)]$
6: $P_G^n(H_s) \leftarrow \text{MPC}(\boldsymbol{c}, \boldsymbol{e})$
7: $L_{PD} = [L_{PD}, (\underbrace{c_G(H_s) + n \cdot \Delta c}_{\text{price}}, \underbrace{P_G^n(H_s)}_{\text{demand}})]$
8: **end for**
9: Construct a block curve based on L_{PD}.

subject to

$$E(h+1) = E(h) - \Delta H \cdot P_E(h) - \Delta H \cdot |P_E(h)| \cdot (1 - \sqrt{\eta}) \tag{22}$$

$$P_G(h) \cdot \Delta H + P_E(h) \cdot \Delta H = E_W(h) \tag{23}$$

$$P_G(h) \geq 0 \tag{24}$$

$$E^{\min} \leq E(h) \leq E^{\max} \tag{25}$$

$$-P_E^{\max} \leq P_E(h) \leq P_E^{\max} \tag{26}$$

$$\Delta H \cdot P_E(h) \cdot (2 - \sqrt{\eta}) \leq E(h) - E^{\min} \tag{27}$$

$$-\Delta H \cdot P_E(h) \cdot \sqrt{\eta} \leq E^{\max} - E(h), \tag{28}$$

where $P_G(h)$ denotes the power drawn from the grid at hour h. H_s and H_P denote the starting hour and the prediction horizon, respectively. $c_G(h)$ is the LMP forecast at hour h. $E(h)$ denotes the remaining energy of the ESS at hour h. $E^{\min}$ and $E^{\max}$ are the lower bound and the upper bound of $E(t)$, respectively. η denotes the round-trip efficiency of the ESS. $P_E(h)$ denotes the output power of the ESS at hour h. $P_E^{\max}$ is the maximum output power of the ESS. The objective function (21) calculates the entire energy cost within the prediction horizon. Eq. (22) describes the dynamics of the ESS. Note that the last term on the right hand side represents the energy loss caused by charging/discharging. Eq. (23) ensures the conservation of energy. (24) indicates the energy that cannot be sold back to the grid. (25) defines the lower and upper bounds of the remaining energy of the ESS. (26) defines the range of the ESS output power. (27) ensures the ESS never discharges more than its available energy. (28) ensures the remaining energy of the ESS never exceeds the upper bound. Note this optimization problem is linear except for one absolute value in Eq. (22). This kind of problem can be easily solved through existing commercial solvers, for instance, CPLEX and Gurobi. In this study, we are using Gurobi to solve this optimization problem.

By solving the above MPC problem, we obtain an optimal control sequence of power drawn from the grid within the prediction horizon: $[P_G^0(H_s), \ldots, P_G^0(H_s + H_P - 1)]$. We only keep the first step of the control sequence $P_G^0(H_s)$ and discard the remaining entries. A pair of price and demand $(c_G(H_s), P_G^0(H_s))$ is therefore acquired. By running MPC with multiple modified LMP forecasts at the starting hour H_s, we obtain a list of price–demand pairs, forming the demand bid curve as shown in Fig. 5. Algorithm 1 presents detailed procedures for the proposed demand bid curve construction. First, the LMP forecast and the wireless charging load estimate within the prediction horizon are obtained.

Then we modify the first element in the LMP forecast array by adding $n \cdot \Delta c$, where n loops from $-N_c$ to N_c with a step size of 1. Δc denotes the cost increment that is a constant. The corresponding demand $P_G^n(H_s)$ is acquired by solving the MPC problem with the modified LMP forecast array. After looping through all the modified LMP forecast arrays, we obtain a list of price–demand pairs, based on which the demand bid curve for the starting hour H_s is constructed.

3.4. DCOPF

ISOs and RTOs in the United States adopt OPF-based approaches to settle clearing prices in electricity markets [29]. In this subsection, we present a DCOPF formulation characterized by price-sensitive demand bids. The goal of the proposed DCOPF is to find an optimal dispatch of power generation resources, which maximizes the overall surplus of the customers and the suppliers with all the demands and the physical constraints being satisfied.

$$\underset{G_i, D_i}{\text{maximize}} \quad \sum_{i=1}^{N} g_i(D_i) \cdot D_i - \sum_{i=1}^{N} c_i \cdot G_i \tag{29}$$

$$\text{subject to} \quad \sum_{i=1}^{N} G_i = \sum_{i=1}^{N} D_i \tag{30}$$

$$-P_l^{\max} \le \sum_{i}^{N} PTDF_{l,i} \cdot \left(G_i - D_i\right) \le P_l^{\max}, \qquad \forall l \tag{31}$$

$$D_i \ge 0, \qquad \forall i \tag{32}$$

$$G_i^{\min} \le G_i \le G_i^{\max}, \qquad \forall i, \tag{33}$$

where G_i and D_i denote the power generation offer and power demand bid at node i, respectively. $g_i(D_i)$ is a block curve describing the corresponding price-sensitive demand bid. Note that $g_i(D_i)$ is a constant for a fixed demand bid. c_i denotes the unit cost of generation resource at node i. PTDF is an acronym for power transfer distribution factor. $PTDF_{l,i}$ measures the change in the power flow on line l given a unit of power injection at node i. $P_l^{\max}$ is the capacity of power line l. $G_i^{\min}$ and $G_i^{\max}$ denote the minimum and the maximum output power of the generation resource at node i. The objective function (29) calculates the overall surplus of the power consumers and power suppliers. Eq. (30) ensures the conservation of energy. (31) ensures that the power flow at each power line is within its capacity. (32) and (33) ensure the demand bids and the generation offers are within feasible ranges, respectively.

The optimal dispatch of generation resources and the cleared demand bids are determined by solving the above DCOPF. The LMP at node i is calculated by:

$$LMP_i = \underbrace{\lambda}_{\text{Energy}} + \underbrace{\sum_{l=1}^{N_L} PTDF_{l,i} \cdot \mu_l^+ + \sum_{l=1}^{N_L} -PTDF_{l,i} \cdot \mu_l^-}_{\text{Congestion}}, \tag{34}$$

where N_L is the number of power lines in the power network. λ is the dual variable for the equality constraint (30). μ_l^+ and μ_l^- are the dual variables for the inequality constraints (31). Note that the LMP at a node can be divided into two components. The first component is the energy cost that equals λ. The second component is the congestion cost that depends on PTDF, μ_l^+, and μ_l^-. Although the energy cost is the same across the power network, LMPs at different nodes can be different due to different congestion costs. If there is no congestion in the power network, then LMPs at all the nodes will be the same. Note that the cost of energy loss during transimission is ignored in this formulation.

4. Numerical example

We validate the performance of the proposed approach based on a simulation study in this section. We first describe the simulation settings and introduce our data sources. Then, we evaluate our LMP forecasting performance by comparing the proposed GSP-based LMP forecasting model with two baseline models. Next, we investigate the performance of wireless charging load estimation using the proposed dynamic traffic flow model. Finally, we demonstrate that the proposed bidding strategy outperforms a baseline bidding strategy in terms of energy costs for operating the wireless charging roads.

Note carrying out a real-world experiment would be extremely expensive, for example, a pilot project in Gotland is expected to cost $12 million to deploy coils across 2.5 miles of road [30]. Meanwhile, real-world test of the integration of wireless charging roads into the existing power market will be a large scale project that involves multiple stakeholders as well as their intensive efforts, which is out of our scope at the current stage.

Table 1
Parameters of the road network connecting five load centers.

Direction	Capacity (veh/h)	Free-flow time (hr)	Wireless charging
1→2	300	3	No
1→4	400	2	Yes
1→5	500	4	Yes
2→1	300	3	No
2→3	300	3	No
2→4	600	2	Yes
3→2	300	3	No
3→5	400	2	No
4→1	400	2	Yes
4→2	600	2	Yes
4→5	500	3	No
5→1	500	4	Yes
5→4	500	3	No
5→3	400	2	No

Table 2
O–D matrix for the road network connecting five load centers.

Load center	1	2	3	4	5
1	0	150	200	380	460
2	150	0	150	420	100
3	200	150	0	200	200
4	350	380	200	0	200
5	280	100	200	200	0

4.1. Simulation settings and data sources

In this numerical example, we study the coupled transportation–power system as illustrated in Fig. 11, where five load centers are connected by a road network that consists of both normal roads and wireless charging roads. The corresponding power network is comprised of eight nodes, three of which represent the wireless charging roads with energy storage. The minimum and maximum remaining energy of each ESS ($E^{\min}$ and $E^{\max}$) are 5 MWh and 25 MWh, respectively. The maximum output power of each ESS ($P_E^{\max}$) is 5 MW.

Every road in this study is assumed to be a two-way street. Table 1 presents the parameters of the road network. Each row provides us information about one direction of a road, which includes its direction, capacity, free-flow time, and wireless charging lane availability. Throughout this study, 25% and 75% capacities of each wireless charging road are assigned to its wireless charging lanes and normal lanes, respectively, for both directions. The wireless charging power is 20 kW per EV. Note that traffic flow into a road changes over time in a real-world road network. To simulate this variation, we set the traffic flow into a road at any time step as a product of a base flow value and a scale factor. Table 2 shows an origin–destination (O–D) matrix for our road network, which provides the base value of traffic flow into each road by solving a static traffic assignment [31] at each hour. The scale factors are obtained by normalizing a reference flow curve via dividing by the mean. We collect ten-week data (from Jun. 7 to Aug. 15, 2016) on Yellow Cab trips in New York City [32] as the reference

Table 3
Capacities of power lines.

Power line	1–2	1–5	2–3	3–5	4–5	1–6	6–4	2–7	7–4	1–8	8–5
Capacity (MW)	80	200	100	150	60	50	50	50	50	50	50

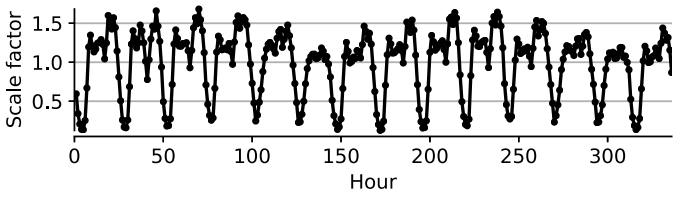

Fig. 6. First two week of the scale factors derived from the reference flow curve.

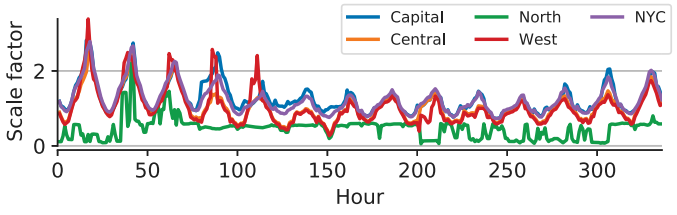

Fig. 7. First two week of the scale factors derived from the five reference cost curves.

flow curve. Fig. 6 displays the first two week of the scale factors derived from the reference flow curve. Clearly the traffic is always heavier during daytime hours than at night. The morning and evening rush hours correspond to the scale factor curve's peaks during weekdays.

As depicted in Fig. 1(b), the corresponding power network consists of eight nodes, which are connected by the power lines. Table 3 provides the capacity of each power line, where i–j refers to the power line that connects load centers i and j. Nodes 1–5 represent five load centers in the power network. Each load center has a power plant with a minimum output power of 10 MW. The maximum output powers of these five power plants are 150 MW, 200 MW, 150 MW, 300 MW, and 250 MW, respectively. The generation costs of power plants in the real world can vary with time. To simulate this variation, we set the unit cost of energy generated by a power plant as a product of a base cost value and a scale factor. The base cost values for these five power plants at nodes 1–5 are 35 $/MWh, 20 $/MWh, 30 $/MWh, 15 $/MWh, and 40 $/MWh, respectively. The scale factors are derived by normalizing reference cost curves via dividing by the mean. In this study, we collected ten-week hourly LMP data (from Jun. 7 to Aug. 15, 2021) of five power plants located in the capital region, central region, northern region, western region, and New York City region of New York State [33] as the reference cost curves. Fig. 7 shows the first two week of the scale factors derived from these five reference cost curves. Clearly, the generation costs can change significantly over time.

Similarly, the electric load of a load center also changes with time. To simulate this variation, we set the electric load of a load center as a product of a base load value and a scale factor. The base load values for load centers 1–5 are 100 MW, 150 MW, 100 MW, 120 MW, and 150 MW, respectively. The scale factors at different hours are obtained by normalizing reference load curves via dividing by the mean. We collected ten-week hourly load data (from Jun. 7 to Aug. 15, 2021) for five zones (Capital, Central, North, West, and New York City) in New York State [34] as the reference load curves for load centers 1–5, respectively. Fig. 8 displays the first two week of the scale factors derived from these five reference load curves. A clear daily pattern is observed in each load profile.

We also collected ten-week (from Jun. 7 to Aug. 15, 2021) historic temperature measurements recorded by five weather stations located in the capital region, central region, northern region, western region,

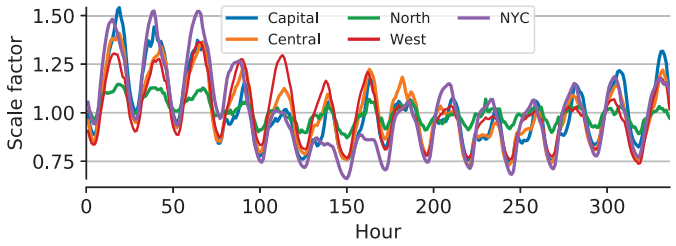

Fig. 8. First two week of the scale factors derived from the five reference load curves.

and New York City region of New York State from weather.com [35]. Note that the temperature data are required in LMP forecasting.

4.2. LMP forecasting performance

In this subsection, we evaluate the performance of the proposed LMP forecasting model by comparing it with that of two baseline models. Given there exists a strong daily pattern in the LMP data, the first baseline model is a seasonal vector autoregressive (VAR) model with seasonal period $S = 24$. This model includes a non-seasonal autoregressive (AR) component at lag 1 and a seasonal autoregressive component at lag 1, which is expressed by the following equation:

$$(1 - \boldsymbol{\Phi}_1 B)(1 - \boldsymbol{\Psi}_1 B^{12})\boldsymbol{y}(h) = \boldsymbol{\epsilon}(h), \tag{35}$$

where B denotes the lag operator. $\boldsymbol{\Phi}_1$ is the coefficient matrix of the non-seasonal AR(1) term. $\boldsymbol{\Psi}_1$ is the coefficient matrix of the seasonal AR(1) term. Note that an equivalent form of this VAR model can be written as:

$$\boldsymbol{y}(h) = \boldsymbol{\Phi}_1 \boldsymbol{y}(h-1) + \boldsymbol{\Psi}_1 \boldsymbol{y}(h-24) + (-\boldsymbol{\Phi}_1\boldsymbol{\Psi}_1)\boldsymbol{y}(h-25) + \boldsymbol{\epsilon}(h). \tag{36}$$

The above equation describes a vector autoregressive model with predictors at lags 1, 24, and 25. The coefficient matrices can be estimated through maximum likelihood estimation. We name the first baseline model S-VAR.

The second baseline model is identical to the proposed regression model except for the modeling of the error terms. Instead of the proposed GSP-based approach, a VAR model is employed to spatio-temporally model $\boldsymbol{\epsilon}(h)$:

$$\boldsymbol{\epsilon}(h) = \boldsymbol{\Gamma}_1 \boldsymbol{\epsilon}(h) + \boldsymbol{\Gamma}_2 \boldsymbol{\epsilon}(h-24) + \boldsymbol{\omega}(h), \tag{37}$$

where $\boldsymbol{\Gamma}_1$ and $\boldsymbol{\Gamma}_2$ are coefficient matrices consisting of parameters that can be estimated through maximum likelihood estimation. $\boldsymbol{\omega}(h)$ denotes the residual term. The AR term at lag 24 is introduced to capture the 24-hour periodicity existing in the error terms. We call the second baseline model VAR-Error. In this numerical example, the error vector $\boldsymbol{\epsilon}(h)$ has a dimension of 8. Therefore, $\boldsymbol{\Gamma}_1$ and $\boldsymbol{\Gamma}_2$ have 64 parameters in each, summing up to a total number of 128 parameters in this case. These parameters need to be fitted with historical data.

Note that we concentrate on evaluating the LMP forecasting performance in this subsection. To simplify our study, we assume there is no ESS associated with any wireless charging road. The hourly traffic flow on each road is obtained through traditional static traffic assignment [31]. The wireless charging roads have to draw an exact amount of power from the grid to satisfy the charging demand of EVs. The LMPs at different nodes in the power network are obtained by solving DCOPF for each hour within the simulation horizon.

Table 4
Average RMSEs of LMP forecasting.

Node	1	2	3	4	5	6	7	8	Mean
Proposed ($)	15.42	15.20	16.48	15.44	20.76	15.81	16.54	15.54	16.40
VAR-Error ($)	15.83	15.59	17.24	16.16	21.47	16.25	17.28	16.24	17.01
S-VAR ($)	52.95	64.05	57.00	53.62	53.71	60.77	53.49	52.91	56.06

Table 5
Average MAPEs of LMP forecasting.

Node	1	2	3	4	5	6	7	8	Mean
Proposed (%)	29.33	32.38	33.42	33.14	36.85	31.23	29.73	32.95	32.38
VAR-Error (%)	29.86	33.22	33.42	34.47	36.80	32.29	30.84	34.70	33.20
S-VAR (%)	49.63	63.11	52.64	50.25	50.11	52.19	49.37	53.44	52.59

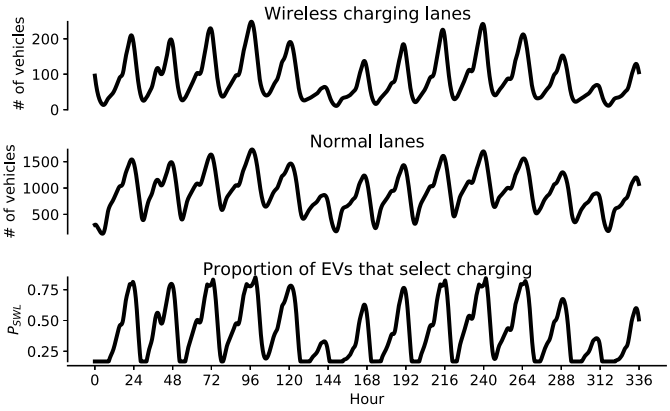

Fig. 9. Performance of the proposed dynamic traffic flow model.

We carry out a rolling forecast test to evaluate the forecast accuracy for each model, a method widely adopted in previous studies [36–38]. The training window size for both the proposed model and the baseline models is one week. The testing window size is the same as the prediction horizon, which is 24 h. The training window slides one day forward after each iteration in the rolling forecast tests. For each iteration, one week of LMP data in the current training window are used to fit the models, the performances of which are evaluated in the following one-day testing data. It is worth noting that the LMP data are standardized using a z-score during each training process. We measure the forecast performance by calculating the corresponding average root mean square errors (RMSEs) and average mean absolute percentage errors (MAPEs). Tables 4 and 5 present average RMSEs and average MAPEs of each model for different nodes in the given power network. Clearly, the proposed approach outperforms the baseline models in terms of both RMSE and MAPE. The proposed method achieves a higher forecast accuracy because it better captures the intrinsic properties of the error terms. The VAR-Error model is more likely to overfit the error terms due to its relatively large number of parameters. Nonetheless, the performance difference between these two methods is small and both of them achieve significantly higher accuracy than the S-VAR model. The reason that S-VAR model performs worse than the other two models is because it is a pure autoregressive model, specifying that the output vector depends linearly on its own previous values and a stochastic error vector term. S-VAR model does not require additional covariates such as temperature or time index, making it more generally applicable. However, due to the lack of information from independent variables as well as the neglect of error vector during forecast, S-VAR is likely to achieve lower accuracy than the other two models.

4.3. Wireless charging load estimation performance

In this subsection, we investigate the performance of wireless charging load estimation using the proposed dynamic traffic flow model. The simulation time interval ΔT is 0.1 h. Recall that the hourly traffic flows into a road are obtained through traditional static traffic assignment. The traffic flows at time steps between any two adjacent hours are then derived through linear interpolation. The initial values of Q_W and Q_N for each direction of a wireless charging road are:

$$Q_W(0) = 0.5 \cdot T_F \cdot C_W \tag{38}$$

$$Q_N(0) = 0.5 \cdot T_F \cdot C_N, \tag{39}$$

which indicate an initial traffic condition with half the critical density. The charging price for each EV $p_W(t)$ is 15 $/hour at all times. The time of value p_T is 10 $/hour. The bonus value of selecting wireless charging for an EV is 5 $/hour. The hyperparameter $\alpha = 0.2$.

Fig. 9 displays the performance of a two-week traffic simulation for one direction of a wireless charging road using the proposed dynamic traffic flow model. The upper and middle subplots show the number of vehicles on wireless charging lanes and normal lanes ($Q_W(t)$ and $Q_N(t)$), respectively. A clear daily pattern can be observed in both curves. The traffic during daytime hours is heavier than nighttime hours for both wireless charging lanes and normal lanes. Being proportional to the quantity of EVs on the wireless charging lanes, the wireless charging load is therefore significantly larger during daytime, allowing opportunity for energy arbitrage through the ESS. The bottom subplot records the proportion of EVs that choose to enter wireless charging lanes at different hours. Not surprisingly, more EVs will select wireless charging roads if the normal lanes get crowded, thereby increasing the wireless charging load. We are unable to quantitatively measure the performance of the proposed wireless charging load estimation method at now because of unavailability of real-world system and data. Nevertheless, all these patterns observed from this simulation comply with our expectation for traffic conditions of real-world wireless charging roads.

4.4. Energy cost comparison

The primary objective of this study is to provide wireless charging road owners with an efficient demand bidding strategy, or equivalently, a control strategy of ESS that saves their energy costs for providing EV charging services. To validate its effectiveness in cost reduction, we compare the performance of the proposed approach with a naive bidding strategy, which serves as the baseline algorithm.

The adopted naive bidding strategy for each wireless charging road is described as follows:

- Step 1: Calculate the average LMP at each hour in a day based on the historic LMPs of the last seven days.
- Step 2: Discharge the ESS with a fixed output power ($E^{\max} - E^{\min}$)/8 during the eight hours with the highest average LMPs. The corresponding demand bid is a fixed bid that equals the difference between the wireless charging load estimate and the ESS output.

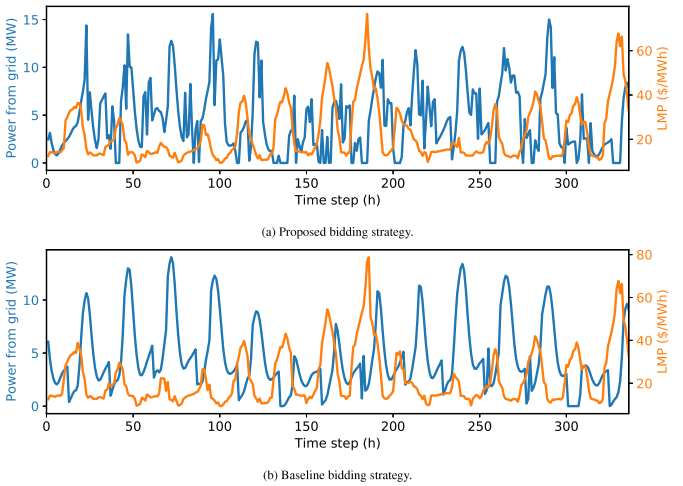

Fig. 10. Grid power drawn by a wireless charging road during the first two weeks of simulation under the proposed and the baseline bidding strategies.

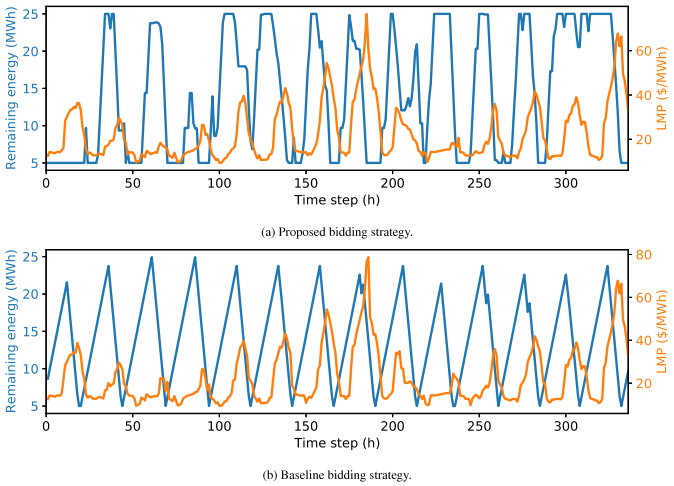

Fig. 11. Remaining energy of a wireless charging road's ESS during the first two weeks of simulation under the proposed and the baseline bidding strategies.

Table 6
Cost comparison between the proposed price sensitive bidding strategy and the baseline bidding strategy.

Charging road	1–4	2–4	1–5	Mean
Proposed ($)	85,034	201,337	158,765	148,379
Baseline ($)	94,070	210,615	169,004	157,896
Percentage saving (%)	9.61	4.41	6.06	6.03

- Step 3: Charge the ESS with a fixed input power $(E^{\max} - E^{\min})/16$ during the remaining 16 h with the lower average LMPs. The corresponding demand bid is a fixed bid that equals the sum of the wireless charging load estimate and the ESS input.

The above three steps are repeated for every testing day. The motivation behind this method is to achieve energy arbitrage by storing electricity during low price period (usually nighttime hours) and release the stored energy for EV charging during peak hours when the price rises. This simple yet effective strategy of storing energy during off-peak hours is popular among electricity cost-saving studies using ESSs [39].

We simulate the electricity market clearing process for nine weeks based on the simulation settings and the data sources introduced in Section 4.1. The first week of data are used for initial training of the proposed LMP forecasting model. Table 6 compares the entire energy costs using the proposed price-sensitive bidding strategy and the baseline bidding strategy for each wireless charging road in our 9-week simulation study. The proposed approach yields lower energy costs for all three wireless charging roads. On average, a 6% cost saving is achieved by replacing the baseline bidding strategy with the proposed price sensitive bidding strategy.

The left side y-axes of Figs. 10(a) and 10(b) display the grid power drawn by a wireless charging road in the first two weeks of simulation under the proposed bidding strategy and the baseline bidding strategy, respectively. The right side y-axes present the corresponding LMPs. Clearly, both bidding strategies tend to bid more quantity when the electricity price is lower. The baseline bidding strategy yields a more regular daily pattern due to its naive bidding rules. Figs. 11(a) and 11(b) show the remaining energy of a wireless charging road's ESS during the first two weeks of simulation under the proposed and the baseline bidding strategies, respectively. Both approaches charge the ESS when the LMP is relatively low and discharge the ESS to serve the wireless charging load when the LMP rises for each day. Similarly, the baseline bidding strategy gives a more regular daily pattern due to its naive rule-based algorithm.

Table 7
Grid pressure indicator results.

Indicator	TAM of LMP	TASD of LMP
Proposed ($)	37.200	1.786
Baseline ($)	37.432	1.833

Note that the proposed price-sensitive bidding strategy can help alleviate the power grid pressure. Recall that a LMP is a sum of an energy price and a congestion price. The energy price is the same across the power network. The congestion price varies depending on the congestion level. If no congestion exists in the power network, then LMPs at different nodes will be the same. Therefore, we can use time average of the maximum (TAM) of the LMP and the time average of the standard deviation (TASD) of the LMP within a power network as two indicators of grid pressure [40]. Their formulations are as follows:

$$\text{TAM of LMP} = \frac{1}{T}\sum_{t=1}^{T} \max\left\{LMP_i(t) | i = 1, \ldots, N_b\right\} \tag{40}$$

$$\text{TASD of LMP} = \frac{1}{T}\sum_{t=1}^{T} \sqrt{\frac{1}{N_b}\sum_{i=1}^{N_b}\left(LMP_i(t) - \frac{1}{N_b}\sum_{k=1}^{N_b} LMP_i(t)\right)^2} \tag{41}$$

where N_b denotes the number of buses in a power grid. $LMP_i(t)$ is the LMP at the ith bus at time t. Table 7 presents the results of these two grid pressure indicators. The proposed price-sensitive bidding strategy leads to lower grid pressure compared with the baseline bidding strategy in terms of these two indicators.

5. Conclusion

This paper develops an efficient price-sensitive bidding strategy to reduce electric energy cost for operating a wireless charging road with an energy storage system. The proposed bidding strategy is formulated upon a model predictive control framework, which requires estimates of future LMPs and wireless charging load. In this study, we propose a composite statistical model based on graph signal processing and linear regression to forecast future LMPs. A point queue-based traffic flow model is formulated to simulate the future EV traffic flow, from which the wireless charging load is estimated. Our numerical example demonstrates that the proposed price-sensitive bidding strategy can effectively achieve a 6% energy cost saving on average. Meanwhile, the simulation results indicate the proposed approach not only saves the energy cost but also reduces the grid pressure compared to the baseline bidding strategy.

Given the proposed bidding strategy is based on an MPC framework that takes LMP forecasts and wireless charging load estimates as inputs and outputs an optimal bid-quantity price pair, the performance of the proposed approach is highly dependent on the quality of these two estimates. More accurate predictions of LMP and wireless charging load is likely to yield more energy cost savings as well as grid pressure alleviation. It should be noted all the results shown in this study are based on simulations. Real-world cases can be significantly more complex and involve more uncertainties. The performance can vary case by case depending on the accuracy of charging load estimates and LMP forecasts.

CRediT authorship contribution statement

Jie Shi: Conceptualization, Methodology, Numerical study, Writing – original draft. **H. Oliver Gao:** Conceptualization, Paper design, Supervision, Writing – review & editing.

Declaration of competing interest

The authors declare that they have no known competing financial interests or personal relationships that could have appeared to influence the work reported in this paper.

Data availability

The authors are unable or have chosen not to specify which data has been used.

References

[1] Voelcker J. Range anxiety is very real, new J.D. Power EVs survey finds. 2021, URL https://www.forbes.com/wheels/news/range-anxiety-very-real-jd-power-evs-survey/.
[2] Shi J, Gao Y, Wang W, Yu N, Ioannou PA. Operating electric vehicle fleet for ride-hailing services with reinforcement learning. IEEE Trans Intell Transp Syst 2020;21(11):4822–34.
[3] Villarreal B. EV charging speeds, charging levels, and charging stations: What's the difference?. 2020, URL https://semaconnect.com/blog/ev-charging-speeds-charging-levels-and-charging-stations-whats-the-difference/.
[4] Electreon Projects.
[5] Smartroad gotland. 2022, URL https://electreon.com/projects/gotland.
[6] Arena of the future. 2022, URL https://electreon.com/projects/arena-of-the-future.
[7] Blain L. In-road inductive charging tests demonstrate unlimited EV range. New Atlas 2022. URL https://newatlas.com/automotive/stellantis-road-charging-induction/.
[8] He J, Yang H, Tang T-Q, Huang H-J. Optimal deployment of wireless charging lanes considering their adverse effect on road capacity. Transp Res C 2020;111:171–84.
[9] Ngo H, Kumar A, Mishra S. Optimal positioning of dynamic wireless charging infrastructure in a road network for battery electric vehicles. Transp Res D 2020;85:102385.
[10] Liu H, Zou Y, Chen Y, Long J. Optimal locations and electricity prices for dynamic wireless charging links of electric vehicles for sustainable transportation. Transp Res E 2021;152:102187.
[11] Zhang S, James J. Electric vehicle dynamic wireless charging system: Optimal placement and vehicle-to-grid scheduling. IEEE Internet Things J 2021.
[12] Li C, Ding T, Liu X, Huang C. An electric vehicle routing optimization model with hybrid plug-in and wireless charging systems. IEEE Access 2018;6:27569–78.
[13] Manshadi SD, Khodayar ME, Abdelghany K, Üster H. Wireless charging of electric vehicles in electricity and transportation networks. IEEE Trans Smart Grid 2017;9(5):4503–12.
[14] Ou C-H, Liang H, Zhuang W. Investigating wireless charging and mobility of electric vehicles on electricity market. IEEE Trans Ind Electron 2014;62(5):3123–33.
[15] Xia F, Chen H, Shahidehpour M, Gan W, Yan M, Chen L. Distributed expansion planning of electric vehicle dynamic wireless charging system in coupled power-traffic networks. IEEE Trans Smart Grid 2021.
[16] Conejo AJ, Nogales FJ, Arroyo JM. Price-taker bidding strategy under price uncertainty. IEEE Trans Power Syst 2002;17(4):1081–8.
[17] Fleten S-E, Pettersen E. Constructing bidding curves for a price-taking retailer in the norwegian electricity market. IEEE Trans Power Syst 2005;20(2):701–8.
[18] Jiang DR, Powell WB. Optimal hour-ahead bidding in the real-time electricity market with battery storage using approximate dynamic programming. INFORMS J Comput 2015;27(3):525–43.
[19] Liu Y, Yu N, Wang W, Guan X, Xu Z, Dong B, et al. Coordinating the operations of smart buildings in smart grids. Appl Energy 2018;228:2510–25.
[20] Wei T, Zhu Q, Yu N. Proactive demand participation of smart buildings in smart grid. IEEE Trans Comput 2015;65(5):1392–406.
[21] Vagropoulos SI, Bakirtzis AG. Optimal bidding strategy for electric vehicle aggregators in electricity markets. IEEE Trans Power Syst 2013;28(4):4031–41.
[22] Bessa RJ, Matos M. Global against divided optimization for the participation of an EV aggregator in the day-ahead electricity market. part I: Theory. Electr Power Syst Res 2013;95:309–18.
[23] Bessa RJ, Matos M. Global against divided optimization for the participation of an EV aggregator in the day-ahead electricity market. Part II: Numerical analysis. Electr Power Syst Res 2013;95:319–29.
[24] Yang H, Zhang S, Qiu J, Qiu D, Lai M, Dong Z. Cvar-constrained optimal bidding of electric vehicle aggregators in day-ahead and real-time markets. IEEE Trans Ind Inf 2017;13(5):2555–65.
[25] Zheng Y, Yu H, Shao Z, Jian L. Day-ahead bidding strategy for electric vehicle aggregator enabling multiple agent modes in uncertain electricity markets. Appl Energy 2020;280:115977.
[26] Şengör İ, Çiçek A, Erenoğlu AK, Erdinç O, Catalão JP. User-comfort oriented optimal bidding strategy of an electric vehicle aggregator in day-ahead and reserve markets. Int J Electr Power Energy Syst 2020;122:106194.
[27] Stanković L, Sejdić E. Vertex-frequency analysis of graph signals. Springer; 2019.
[28] Jin W-L, Wang X, Lou Y. Stable dynamic pricing scheme independent of lane-choice models for high-occupancy-toll lanes. Transp Res B 2020;140:64–78.
[29] Yu N, Liu C-C, Price J. Evaluation of market rules using a multi-agent system method. IEEE Trans Power Syst 2009;25(1):470–9.
[30] Krauss C. Electric roads could be a path to a driverless future. NY Times 2019. URL https://www.nytimes.com/2019/10/07/business/energy-environment/electric-roads-cars-israel-sweden.html.
[31] Patriksson M. The traffic assignment problem: models and methods. Courier Dover Publications; 2015.
[32] Yellow taxi trip data. 2016, URL https://data.cityofnewyork.us/dataset/2016-Yellow-Taxi-Trip-Data/uacg-pexx.
[33] New York ISO energy market & operational data. 2021, URL https://www.nyiso.com/energy-market-operational-data.
[34] New york ISO load data. 2021, URL https://www.nyiso.com/load-data.
[35] Weather data. 2021, URL https://weather.com/.
[36] Ma Z, Zhong H, Xie L, Xia Q, Kang C. Month ahead average daily electricity price profile forecasting based on a hybrid nonlinear regression and SVM model: an ERCOT case study. J Mod Power Syst Clean Energy 2018;6(2):281–91.
[37] Zheng K, Wang Y, Liu K, Chen Q. Locational marginal price forecasting: A componential and ensemble approach. IEEE Trans Smart Grid 2020;11(5):4555–64.
[38] Li Y, Yu N, Wang W. Machine learning-driven virtual bidding with electricity market efficiency analysis. IEEE Trans Power Syst 2021.
[39] Mo Y, Lin Q, Chen M, Qin S-ZJ. Online peak-demand minimization using energy storage. 2021, arXiv preprint arXiv:2103.00005.
[40] Shi J, Gao HO. Efficient energy management of wireless charging roads with energy storage for coupled transportation–power systems. Appl Energy 2022;323:119619.